A mechanistic model to predict saturated pool boiling critical heat flux (CHF) in confined geometries

A. A. Alsaati

D. M. Warsinger

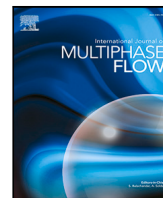Justin A. Weibel
jaweibel@purdue.edu

A. M. Marconnet

A mechanistic model to predict saturated pool boiling Critical Heat Flux (CHF) in a confined gap

Albraa A. Alsaati, David M. Warsinger, Justin A. Weibel, Amy M. Marconnet [*]

School of Mechanical Engineering, Purdue University, West Lafayette, 47907, IN, United States

ARTICLE INFO

ABSTRACT

Boiling enables high rates of heat transfer from a surface made possible at a relatively low thermal resistance motivating the use of two-phase cooling for increasingly compact thermal management solutions. However, extreme geometrical confinement of the liquid above the boiling surfaces is known to have detrimental effects on maximum heat transfer rate by inducing premature onset of film boiling. Moreover, previously developed critical heat flux (CHF) models for confined geometries focused on triggering mechanisms associated with unconfined pool boiling and, thus, are not generalizable. This work proposes a new mechanistic model for predicting CHF during boiling within in narrow gap, specifically developed to account for confinement effects on the triggering mechanism. The model postulates that occurrence of CHF coincides with the irreversible growth of a dry spot on the boiling surface. Three competing forces govern the two-phase interface dynamics, namely vapor momentum, surface tension, and hydrostatic forces. Dryout is triggered when the vapor momentum force due to vaporization at the two-phase interface balances the combined surface tension and hydrostatic forces leading to irreversible growth of the dry spot. The present work offers a predictive confined CHF model that accounts for confined boiling surface shape, size, orientation, confinement gap spacing, and working fluid properties, with a single fluid-specific fitting coefficient that represents the ratio of vapor area to the confinement opening area near CHF conditions. Notably, the developed CHF model is also effective in predicting the threshold gap below which confinement reduces pool boiling CHF. The model is compared to 197 experimentally measured confined CHF data points available from 10 studies in the literature that represent 7 different working fluids and a range of boiling surface inclinations and shapes. The model predicts the confinement-reduced CHF values with a root mean square error of 21%, which is less than half of the error compared to all other available predictive models. This clarification of the triggering mechanism and improved prediction accuracy of CHF, as offered by the current study, will enable broader practical system implementation of compact two-phase cooling technologies.

1. Introduction

The use of the latent heat of vaporization during boiling facilitates the removal of high heat densities while maintaining the boiling surface below operational temperature limits. Therefore, boiling is used in various energy conversion and heat exchanging applications (Liang and Mudawar, 2018a). To meet demands for compact and lightweight thermal management devices, increasing the surface-to-volume ratio of two-phase heat exchangers is advantageous in various industrial and scientific applications (Brandner et al., 2006). There is also growing interest in developing miniature cooling technologies that use passive boiling principles in confined geometries such as thermosyphons (Sundaram and Bhaskaran, 2011), pulsating heat pipes (Bastakoti et al., 2018), immersion cooling (Coles and Herrlin, 2017), and two-phase heat spreaders (Moon et al., 2021).

The ubiquity of pool boiling in many industrial and thermal management applications has motivated researchers for decades to understand and characterize the associated transport processes and limits (Carey, 2020). One of the most important boiling characteristics for two-phase thermal management systems is the critical heat flux (CHF), which represents the maximum heat flux at which nucleate boiling can be sustained; above this limit, a system under constant heat flux condition will transition to film boiling (Liang and Mudawar, 2018a). Operating the system above CHF (*i.e.*, in the film boiling regime) results in a drastic increase in the thermal transport resistance due to the formation of a stable vapor blanket that can lead to a catastrophic temperature rise. Restricting boiling to occur in a narrow gap above the boiling surface, termed 'confined boiling' hereafter, significantly

---

* Corresponding author.
  E-mail address: marconnet@purdue.edu (A.M. Marconnet).

Nomenclature

ΔT_s	Wall Superheat, $T_b - T_{sat}$ (K)
A_b	Boiling Surface Area (m^2)
A_{ei}	Two-phase Evaporation Interface Area (m^2)
A_{gap}	Confinement Gap Area (m^2)
A_v	Vapor Outlet Area (m^2)
D	Horizontal Boiling Surface Diameter (m)
D_{eq}	Equivalent Boiling Surface Diameter (m)
f	Friction Factor (–)
F_G	Hydrostatic Force (N)
F_m	Vapor Momentum Force (N)
F_s	Surface Tension Force (N)
g	Gravitational Acceleration (m/s^2)
H_i	Effective Depth of the Two-phase Interface (m)
h_{lv}	Heat of Vaporization (J/kg)
K	Dimensionless Critical Heat Flux (–)
k_l	Liquid Thermal Conductivity (W/mK)
L	Vertical Boiling Surface Length (m)
L_c	Capillary Length, $\sqrt{\frac{\sigma}{g(\rho_f - \rho_v)}}$ (m)
P_c	Critical Pressure (Pa)
P_d	Dynamic Pressure (Pa)
P_r	Reduced Pressure (–)
q''_b	Average Heat Flux at boiling surface (W/m^2)
$q''_{CHF,Co}$	Confined Critical Heat Flux (W/m^2)
$q''_{CHF,Z}$	Unconfined Critical Heat Flux (W/m^2)
q''_{ei}	Heat Flux at the Two-phase Evaporation Interface (W/m^2)
q''_{pl}	Heat Flux of Unconfined Pool Boiling (W/m^2)
R_a	Average Surface Roughness (m)
S	Confinement Gap Size (m)
S_m	Mean Spacing (m)
t_d	Total Duration for Complete Depletion of the Liquid Layer Underneath the Coalesced Confined Vapor Bubble (s)
t_{ib}	Evaporation Duration (s)
t_s	Bubble Growth Time (s)
u_c	Critical Helmholtz Velocity (m/s)
u_l	Liquid Velocity (m/s)
u_v	Vapor Velocity (m/s)
W	Vertical Boiling Surface Width (m)

Greek Symbols

β	Surface Contact Angle (°)
δ_{ma}	Macrolayer Thickness (m)
ϵ	Perimeter of the Confined Heater (m)
λ_H	Critical Helmholtz Wavelength (m)
μ_l	Dynamic Viscosity (Pa s)
ψ	Vapor Area Ratio at the Confinement Opening Area, $\frac{A_v}{A_{gap}}$ (–)
ρ_l	Liquid Density (kg/m^3)
ρ_v	Vapor Density (kg/m^3)
σ	Surface Tension (N/m)
τ_D	Period of the Vapor Mushroom (s)
θ	Boiling Surface Orientation Angle (°)

from the literature. Notably, the developed CHF model is also effective in predicting the threshold gap below which confinement reduces pool boiling CHF.

2. State-of-the-art models for CHF in confined geometries

The phenomenon of CHF has been experimentally reported since the late 19th century. Lang (1888) experimentally observed that the boiler efficiency in generating steam drastically decreases when the boiling surface superheat reaches a certain limit. Many researchers have since observed the CHF phenomenon and provided further insights into this behavior. However, boiling is a chaotic and a complex two-phase flow phenomenon owing to the dynamic evolution of multiple interfaces covering a wide range of length scales extending from the macroscale down to the molecular level (Theofanous and Dinh, 2006). Therefore, dimensionless groups and empirical constants are often employed in developing correlations useful for engineering applications. Bonilla and Perry (1941) proposed one of the earliest correlations for CHF purely from experimental data. While empirical correlations lack generality and are only applicable in the range of conditions tested, incorporating mechanistic aspects of boiling into such empirical correlations can broaden their range of applicability. For further insights into the mechanisms of CHF refer to the reviews by Liang and Mudawar (2018a,b) for pool boiling; Bruder et al. (2016) and Cheng (2013) for flow boiling; Konishi and Mudawar (2015) for flow boiling in microgravity; and the review by Devahdhanush and Mudawar (2021) for jet impingement boiling. This section discusses theoretical frameworks that have been developed as a basis for a wide range of available models to predict CHF; the specific focus of this brief review is on pool boiling in confined configurations, that is, when the growth of vapor bubbles normal to the boiling surface is interfered with another solid surface before complete detachment of the bubble from the boiling surface, such as due to a parallel plate that forms a narrow gap above the boiling surface.

Geometrical confinement above the boiling surface and/or boiling from heaters of small sizes compared to the bubble dimensions significantly alters the thermofluidic characteristics of pool boiling compared to large surfaces. While there is not yet an agreed upon criterion for the dimension threshold for boiling a liquid in a confined gap above a heated surface, many works compare the gap spacing (or height), S, or the characteristic length of the heater, such as diameter, D, or length, L, to the capillary length of the working fluid, L_c, to define a cutoff where the dimensions alter the pool boiling characteristics. For decades, it has been experimentally observed that confinement reduces the critical heat flux (Katto and Yokoya, 1966; Katto et al., 1977; Misale et al., 2009, 2011; Souza et al., 2013; Kapitz et al., 2019). Significant progress has been made in understanding the underlying mechanism of flow boiling in microchannels where the working fluid is actively

alters the thermofluidic characteristics of pool boiling (Cheng, 2013). Primarily, vapor bubbles are forced to grow parallel to the boiling surface, extending the vapor coverage area associated with each nucleation site, whereas many of the models developed for pool boiling focus on vapor flow normal to the boiling surface. Therefore, the applicability of existing predictive macroscale CHF models needs to be carefully examined to account for these effects of confinement.

This work develops a model to predict CHF that accounts for the mechanistic influence of small gap spacing above the boiling surface, heater size, shape, and orientation on pool boiling. First, a review of the existing confined CHF models is presented. Then, we propose a new model for the CHF during boiling in a confined gap based on the micro-hydrodynamics along the triple contact line on the boiling surface. The accuracy and generality of the developed CHF model, in comparison to previous models, is evaluated against an experimental dataset collected

Table 1

A summary of the dimensionless CHF ratios modified to account for additional factors, $K = \frac{q''_{CHF,Z}}{\rho_v^{0.5} h_{lv} [\sigma g(\rho_l - \rho_v)]^{1/4}}$.

Dimensionless CHF Ratio	Wettability	Pressure	Viscosity	Orientation	Confinement	Reference
Unconfined Pool Boiling						
$K = \pi/24$						Zuber (1959)
$K = \frac{\pi}{16(3)^{1/4}}$						Lienhard and Dhir (1973)
$K = 0.171 \frac{(1+0.324\times10^{-3}\beta^2)^{1/4}}{(0.018\beta)^{1/2}}$	√					Kirichenko and Chernyakov (1971)
$K = 0.0336(\pi-\beta)^3 R_a^{0.125}$	√					Ramilison et al. (1992)
$K = 0.811\left(\frac{1+\cos\beta}{16}\right)\left[\frac{2}{\pi} + \frac{\pi}{4}(1+\cos\beta) + \frac{351.2\cos\beta}{1+\cos\beta}\left(\frac{R_a}{S_m}\right)\right]^{1/2}$	√					Kim et al. (2016)
$K = [0.18 - 0.14(P/P_c)^{5.68}]$		√				Wang et al. (2016)
$K = 0.13 + 4\left[\frac{\rho_l \sigma^{3/2}}{\mu_l^2 [g(\rho_l - \rho_g)]^{1/2}}\right]^{-2/5}$			√			Borishanskii (1955)
$K = 0.131\left[-0.73 + \frac{1.73}{1+10^{-0.02l(185.4-\theta)}}\right] \times \left[1 + \frac{55-\beta}{100}(0.56 - 0.0013\theta)\right]$	√			√		Liao et al. (2008)
$K = [(0.229 - 4.27\times10^{-4}\ \theta)^{-6} + (0.577 - 2.98\times10^{-3}\ \theta)^{-6}]^{-1/6}$				√		El-Genk and Bostanci (2003)
$K = 0.131(1 - 0.001117\theta + 7.79401\times10^{-6}\ \theta^2 - 1.37678\times10^{-7}\ \theta^3)$				√		Arik and Bar-Cohen (2001)
Confined Pool Boiling						
$K = \frac{0.134}{1+6.39\times10^{-5}(\rho_l/\rho_v)^{1.343}P_r^{0.252}(L/S)^{1.517}}$					√	Bonjour and Lallemand (1997)
$K = \frac{0.18}{1+0.00918(\rho_v/\rho_l)^{0.14}[g\frac{(\rho_l - \rho_v)D^2}{\sigma}]^{0.5}(D/S)}$					√	Katto and Kosho (1979)
$K = \frac{0.17}{1+6.8\times10^{-4}(\rho_l/\rho_v)^{0.62}(D_{eq}/S)}$					√	Kim and Suh (2003)
$K = 0.131(0.6028S^{0.3694})$					√	Kim et al. (2020)
$K = 0.185\left(\frac{1}{1+71.43e^{-1.32S}}\right)$					√	Misale et al. (2009)
$K = \frac{0.16}{1+6.7\times10^{-4}(\rho_l/\rho_v)^{0.6}(L/S)}$					√	Monde et al. (1982)

pumped through the confined gaps (Kandlikar, 2012; Harirchian and Garimella, 2009). However, less is understood about the mechanism of CHF during pool boiling in confined geometries, where the vapor bubbles must depart the surface by buoyancy (Cheng, 2013). Although many experimental studies have characterized the effect of geometrical confinement on pool boiling, a predictive correlation for CHF that can be applied to wide range of heater sizes, orientations, gap spacings, and working fluids has not yet been developed (Cheng, 2013).

A common approach taken to predict the CHF for confined boiling is to modify models originally developed for unconfined pool boiling with factors that account for the effect of confinement. The seminal work of Zuber (1959) formulated one of the most widely adopted theoretical frameworks for predicting the CHF for unconfined pool boiling from large flat surfaces. This hydrodynamic theory postulates that vapor generated at the boiling surface forms a periodic array of vapor jets, and that the CHF occurs when the liquid–vapor interfaces of these jets become unstable and block liquid supply back to the boiling surface. Using the critical Helmholtz velocity (Taylor, 1950) as the instability criteria, Zuber (1959) proposed the following relation for CHF, $q''_{CHF,Z}$:

$$\frac{q''_{CHF,Z}}{\rho_v^{0.5} h_{lv} [\sigma g(\rho_l - \rho_v)]^{1/4}} = K, \tag{1}$$

where K is constant, hereafter referred to as the dimensionless CHF ratio. The original work (Zuber, 1959) proposed $K = \frac{\pi}{24}$, for finite surface. Later, Lienhard and Dhir (1973) refined the model to show that a value of $K = \frac{\pi}{16\ (3)^{1/4}}$ was more accurate for flat boiling surfaces much larger than the Helmholtz unstable wavelength.

Despite being perhaps the most common model developed to date, the generalizability of Zuber's CHF prediction has been criticized (Chang, 1957; Lienhard and Dhir, 1973; Lienhard et al., 1973; Theofanous and Dinh, 2006) because it does not account for pressure, surface conditions, viscosity, and wettability despite experimental data suggesting that all of these factors have a strong influence on the CHF. Nevertheless, owing to the success of the underlying hydrodynamic instability theory in predicting CHF in pool boiling, subsequent investigations (Kirichenko and Chernyakov, 1971; Ramilison et al., 1992; Kim et al., 2016; Wang et al., 2016; Borishanskii, 1955; Liao et al., 2008;

El-Genk and Bostanci, 2003; Arik and Bar-Cohen, 2001) attempting to resolve these effects on CHF typically adapted Zuber's framework by including additional empirical factors in the dimensionless CHF ratio, K. The first portion of Table 1 summarizes those modifications for unconfined configurations.

Similarly, this hydrodynamic instability theory has been commonly reused as a framework for CHF predictions that accounts for the confinement effect (Bonjour and Lallemand, 1997; Katto and Kosho, 1979; Kim and Suh, 2003; Kim et al., 2020; Misale et al., 2009; Monde et al., 1982). The second portion of Table 1 summarizes empirical correlations have been developed for the dimensionless CHF ratio, K, as a function of the confinement gap spacing, S, channel length, L, and heater diameter, D. However, it is crucial to revisit the underlying assumptions taken in developing these CHF models based on the hydrodynamic instability theory to reassess their generalized applicability for confined boiling configurations.

The hydrodynamic instability framework idealizes the vapor flow morphology as being large vapor columns normal to the boiling surface. Further, these vapor columns are assumed to arrange in a rectangular array on the boiling surface, as depicted in Fig. 1a, where the array spacing is equal to the dominant unstable Taylor wavelength which was derived by Bellmann and Pennington (1954) to be $\lambda_H = 2\pi(3\sigma/[(\rho_l - \rho_v)g])^{1/2}$. Vapor columns diameters were further assumed be half of the vapor column spacing. The CHF occurs when the average vapor velocity, u_v is equal to the critical Helmholtz velocity, u_c, (Zuber, 1959):

$$u_c = \left[\frac{2\pi\sigma}{\rho_v \lambda_H}\right]^{1/2}. \tag{2}$$

Using energy and mass conservation, the average vapor velocity, u_v, is

$$u_v = \frac{16\ q''_{CHF,Z}}{\pi \rho_v h_{lv}}. \tag{3}$$

Combining Eqs. (2) and (3) leads to the CHF correlation in Eq. (1). While this idealization is rational (albeit disputed) for unconfined conditions, as illustrated in Fig. 1b, the existence of a confinement wall above the boiling surface would surely prohibit the formation
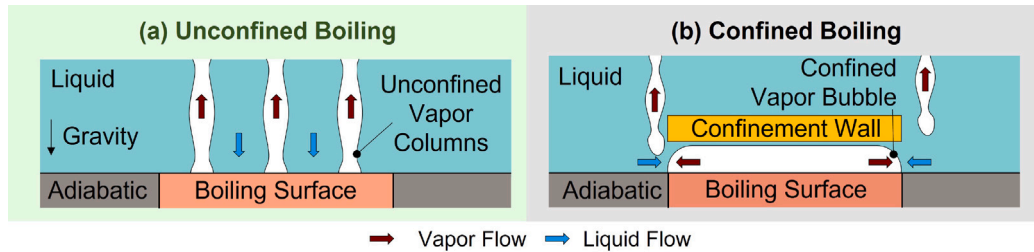
Fig. 1. Two-phase interface dynamics comparison during unconfined and confined pool boiling. (a) Illustration of the theoretical framework for the hydrodynamic instability theory for predicting CHF in saturated pool boiling on an infinite unconfined flat plate. The CHF is postulated to occur when the two-phase interfaces of the unconfined vapor columns are unstable based on the Helmholtz criterion. (b) Illustration of the effect of a confinement wall above a horizontal boiling surface on the two-phase interface dynamics. Instead of forming vapor columns normal to the surface, vapor bubbles are forced to grow parallel to the boiling surface. In both panels, arrows indicate the liquid (blue) and vapor (red) flow paths. (For interpretation of the references to color in this figure legend, the reader is referred to the web version of this article.)

of such vapor columns normal to the boiling surface. As a result, the mechanism of CHF for confined pool boiling is expected to differ significantly.

Several studies develop alternative approaches for predicting the CHF for confined pool boiling that do not use hydrodynamic instability frameworks. Change and Yao (1993) investigated the CHF phenomena in confined geometries by conducting experiments on a vertical cylindrical heater confined by a concentric tube where the bottom opening is sealed and the fluid can access the confinement cavity from the top opening only. In contrast to confined CHF models in Table 1, their developed confined CHF model is based on the well-established understanding of hydrodynamic countercurrent flooding in tubes, namely, the (Wallis, 1969) correlation for countercurrent flooding. The final form of the confined CHF prediction based on the countercurrent flow framework is

$$\frac{q''_{\text{CHF,Co}}}{\rho_v h_{\text{fg}}} \sqrt{\frac{\rho_v}{g D(\rho_l - \rho_v)}} = \frac{0.38}{(1 + (\rho_v/\rho_v)^{0.25})^2 (L/S)}. \tag{4}$$

In this configuration, gravity pulls the liquid down while buoyancy lifts the vapor up. The flooding phenomenon was best described as a transition from counter-current flow to a co-current flow, where the vapor flow reverses the flow direction of a fraction of the liquid entering the cavity (Ragland and Ganic, 1983). While this framework is specifically tailored to the two-phase flow regimes expected in confined configurations, the chosen CHF triggering mechanism, countercurrent flooding, contradicts the experimental observations by others (Alsaati et al., 2021; Bonjour and Lallemand, 1998; FujitaO et al., 1988), which have shown that during confined boiling the heated surface partially dries out at high heat fluxes just before reaching the CHF condition. In other words, liquid only rewets regions near the confined heater perimeter, such that the interior regions of the gap further away from the perimeter are solely occupied by vapor. Chyu (1988) also developed a confined CHF model not based on the hydrodynamic instability theory. Rather, their analysis was based on a one-dimensional momentum conservation of the two-phase flow in narrow vertical channels. Their analysis postulated that the CHF occurs when the buoyancy driven upward momentum is insufficient to balance the momentum of the displaced liquid and associated frictional forces. The expression CHF was derived to be

$$q''_{\text{CHF,Co}} = \rho_v h_{\text{lv}}(S/L) \left[\frac{g L \sin\theta (\rho_l/\rho_v - 2)}{1 + f L/(2S)} \right]^{0.5}, \tag{5}$$

where L is the channel length and f is the friction factor defined as

$$f = 0.13 \left(\frac{\rho_l - \rho_v}{\rho_v} \right)^{0.5} \left[s \left(\sqrt{g \frac{\rho_l - \rho_v}{\sigma}} \right) \right]^{1.3}. \tag{6}$$

While such a friction-based framework is suitable for vertical channels, where the buoyancy drives the vapor flow upward and liquid is supplied from the bottom inlet to the channel, it is challenging to extrapolate this framework into horizontal confined surfaces that have

no clear distinction between liquid inlet and vapor outlet along the confinement perimeter. In contrast to earlier semi-empirical models, Zhao et al. (2001) developed an analytical model for the confined CHF based on the depletion rate of the liquid microlayer underneath the confined bubble,

$$q''_{\text{CHF,Co}} = \frac{q_{\text{pl}}(t_{\text{ib}} + t_s) + \int_{t_{\text{ib}}+t_s}^{t_d+t_s} \frac{k\Delta T_s}{\delta_{\text{ma}}}}{\tau_D}, \tag{7}$$

where q_{pl} is the heat flux of the unconfined pool boiling, t_d, t_{ib}, and t_s are, respectively, the total duration for the complete depletion of the microlayer underneath the coalesced confined vapor bubble, the microlayer evaporation duration at the critical thickness and the bubble growth time as the bubble reaches the confinement wall, δ_{ma} is the microlayer thickness, and ΔT_s is the boiling surface superheat. The analysis considered that the confinement wall forces the individual vapor bubbles to grow parallel to the boiling surface resulting in coalescence and formation of a vapor 'mushroom' inside the confined space, where τ_D is the period of the vapor mushroom formation. This approach is impractical for engineering applications because many of terms in Eq. (7) cannot be quantified *a priori* for a given confined boiling configuration.

3. CHF model development

The literature review above identified the lack of a mechanistic CHF correlations for confined boiling configurations that can be readily applied to across a wide range of parameters. The gap in the literature motivates this work to develop a model to predict CHF that uses a valid triggering mechanism in confined boiling configurations. Generally, the boiling process consists of a various energy transport process coupled with the flow hydrodynamics. Energy needs to transfer across the solid–liquid interface, through the liquid, and across the liquid–vapor interface; generated vapor must flow away while liquid rewets the boiling surface. Interruptions of any of these individual transport mechanisms would act to limit the overall boiling transport as well. Further, the specific boiling system configuration may determine which of these transport mechanisms is the rate-limiting factor. Hence, models for the CHF generally postulate that one of the transfer mechanisms is the weak link when developing the model framework (Carey, 2020). Scattering of thermal energy carriers (phonons) across the solid–liquid interface (e.g., the Kapitza resistance) is unlikely to be the limiting transport mechanism (Pham et al., 2013; Pollack, 1969). Similarly, the maximum possible vapor flux, and associated heat transfer rate, across the liquid–vapor interface based on kinetic theory is typically much larger compared to the other transfer mechanisms (Gambill and Lienhard, 1987). Thus, researchers have historically attributed the limit to hydrodynamic mechanisms, either focusing on the far-field vapor–liquid counterflow or the near-surface liquid delivery to the evaporating contact line (Carey, 2020).

Our past experiments, Alsaati et al. (2021), were analyzed to elucidate the mechanisms that impact the heat transfer coefficient and
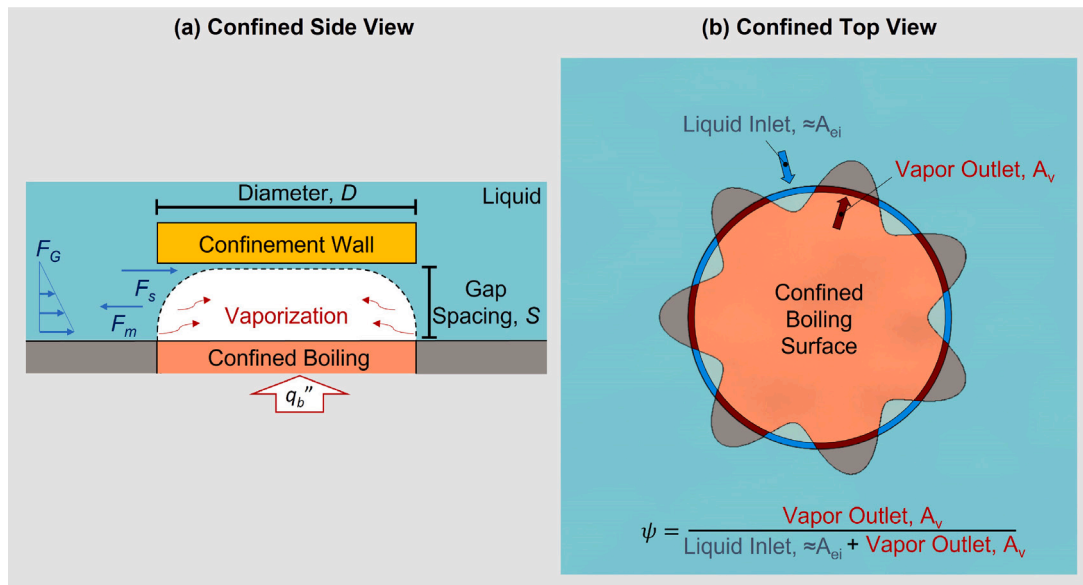
Fig. 2. Micro-hydrodynamics at the contact line as the governing mechanism for CHF in confined geometries (a) Side-view schematic of the cross-section of the confined boiling system where a bubble is growing within a gap spacing, S, from the boiling surface of a diameter, D. Forces governing the two-phase interface dynamics are illustrated with blue arrows. These include the hydrostatic forces, F_G, surface tension forces, F_S, and the vapor momentum forces, F_m. (b) Cross-sectional top view of the base of the confined vapor bubble just prior to CHF. Undulations in the perimeter of the bubble extend partially outside the confined boiling region allowing partial rewetting of the boiling surface near the confinement space perimeter (*i.e.*, the liquid inlet regions). The ratio of the vapor outlet regions (shown in red) to the full perimeter of the boiling surface (combined red and blue line), defined as ψ, is the single fitting parameter in our newly developed correlation. It is worth noting that the actual confined bubble might not be as regularly shaped as the idealized depiction in the figure. However, the definition of the demonstrated fitting parameters, ψ, is still valid for irregular shapes. Refer to Appendix B for an illustration of the model order reduction. (For interpretation of the references to color in this figure legend, the reader is referred to the web version of this article.)

revealed that confined boiling surfaces exhibit partial dryout well below CHF. This experimental observation is also confirmed by Bonjour and Lallemand (1998), FujitaO et al. (1988). In other words, liquid does not rewet the entire boiling surface. Further, the fraction of the surface experiencing partial dryout qualitatively increases as the heat flux increases near the CHF condition. Therefore, the triggering mechanism for CHF in confined configuration should consider the near-surface micro-hydrodynamic forces around the triple contact line. In fact, this mechanism is argued to be the triggering mechanism even for unconfined pool boiling. Theofanous and colleagues (2006, 2002a,b) challenged the widely held view that the hydrodynamic instability is the triggering mechanism for pool boiling CHF and postulated that CHF is triggered when the forces along the triple contact line are balanced, leading to irreversible growth of a dry spot area on the boiling surface. Kandlikar (2001) also used a similar approach to develop a model for unconfined CHF that accounts for both surface wettability and orientation. The work of Theofanous and Dinh (2006) and Kandlikar (2001) inspired the development of the model herein for predicting CHF in confined configuration.

In contrast to pool boiling, confined boiling is less sensitive to bulk thermal hydraulics of the pool. The bulk fluid flow in unconfined pool boiling can interfere with the microscale hydrodynamics near the boiling surface. As depicted in Fig. 1, the bulk fluid supply to the boiling surface results in patches of dry out spots on the unconfined boiling surface. Furthermore, the location of the dry spots fluctuates chaotically across the boiling surface (Bucci et al., 2016). Hence, it is very challenging to account for dry spot fluctuation in predictive CHF model. On the other hand, the confinement wall restricts the thermofluidic interactions between the boiling surface and the working fluid to a microscale layer on the boiling surface perimeter. Thus, the CHF triggering mechanism in confined boiling should be sought at the micro-hydrodynamics at the triple contact line on the boiling surface rather than the pool-thermal-hydraulics. Furthermore, the understanding gained from the micro-hydrodynamics in confined boiling can be leveraged to build a more complex CHF model for unconfined pool boiling where the effect of bulk fluid flow is added.

Considering this triggering mechanism for CHF in confined boiling, a predictive model must consider the forces acting on the two-phase interface. Fig. 2a depicts the forces considered in the model developed herein. Namely, surface rewetting is assumed to be governed by a balance between the surface tension force, F_S, the hydrostatic force, F_G, and the vapor momentum force, F_m (also known as the vapor recoil forces). At low heat fluxes, both hydrostatic and surface tension forces can overcome the vapor momentum force allowing for complete rewetting of the boiling surface. On the other hand, as the applied heat flux increases, the vapor momentum force due to evaporation becomes larger than the combined hydrostatic and surface tension forces forming a partial dry patch at inner most region of confined space. The average equilibrium spread of the region experiencing partial dryout grows irreversibly proportional to the average applied heat flux until it encompasses the entire heater area, leading to a boiling crisis at the CHF condition. Furthermore, the two-phase interface is assumed to undergo unstable undulations along its perimeter, as illustrated in Fig. 2b. Just prior to CHF, the two-phase undulation is assumed to be at the heater perimeter where only a portion of the two-phase interface is in contact with the boiling surface. In the model developed below, it is important to note that the heater surface is assumed to entirely cover one side of the confinement gap while the opposing confinement wall is assumed to be adiabatic, as shown in Fig. 2.

The two-phase interface where vapor generation occurs in the confined region is assumed to be at quasi-steady state. As depicted in Fig. 2, the vapor generation grows the confined bubble to be extend partially outside the confined boiling region. The two-phase interface at the extended volume of the bubble outside of confined region is expected to have larger radius of curvature compared the two-phase interface within the confinement region. In addition, the buoyancy forces are unrestricted by the confinement wall. Hence, the bubble is expected to grow disproportionally at a higher rate at the two-phase interfaces outside of the confinement region. Therefore, near CHF conditions, the vapor generation velocity in confined gaps is assumed to be much higher than the two-phase interface velocity in the confined region.

Vapor momentum forces the contact line to recede and can be evaluated based on the dynamic pressure, P_d, of the vapor phase:

$$P_d \approx 1/2\rho_v u_v^2. \tag{8}$$

Assuming that all of the heat is dissipated by the latent heat of vaporization, the vapor velocity is

$$u_v = \frac{q''_{ei}}{\rho_v h_{lv}}, \tag{9}$$

where q''_{ei} is the heat flux at the evaporation interface, which can be expressed as $q''_{ei} = \left(q''_b A_b\right)/A_{ei}$ where the subscript b indicates heat flux based on the area of the boiling surface. Overall, the vapor momentum forces, F_M, are evaluated as the product of the dynamic pressure, P_d, and the area of the two-phase evaporation interface, A_{ei}, which depends on its shape of the two-phase interface and is an unknown. However, occurrences of viscous fingering (or Saffman-Taylor) instability has been reported in confined boiling configurations (Kapitz et al., 2015). The parameter A_{ei} approximately represents the projected area of the wet fingers into the inlet/outlet opening. Furthermore, the shape of the viscous fingering instability is strongly influenced by the density ratio of the two phases and the capillary number (the relative measure between viscous and surface tension) (Anjos et al., 2017). Therefore, for a given working fluid, the evaporation interface area, A_{ei}, at CHF is assumed to be linearly correlated with the confinement inlet-outlet opening area to the unconfined reservoir, A_{gap}. Further, the two-phase evaporation interface area is approximated to be equal to the liquid inlet area at the confinement opening. A correlation parameter, $(1 - \psi)$, is hence introduced and represents the ratio of the evaporation interface area to the confinement opening area, $(1 - \psi) = A_{ei}/A_{gap}$. This ratio is assumed to be dependent on the working fluid properties only. Combining the equations above results in the following expression for the vapor momentum force:

$$F_m = \frac{q''^2_b A_b^2}{2\rho_v h_{lv}^2 A_{gap}(1 - \psi)}. \tag{10}$$

At the CHF condition, the model postulates that the vapor momentum forces are balanced by surface tension and hydrostatic pressure. Surface tension acts at the three-phase contact lines of the confined vapor. Because the confinement wall is adiabatic, we assume that no evaporation takes place from the top two-phase interface of the confined vapor bubble. Hence, a liquid layer over the confinement wall is preserved and not depleted at CHF (i.e., the confinement wall remains completely wetted). This assumption agrees with visual observations from our previous work (Alsaati et al., 2021). On the other hand, the evaporating liquid microlayer on the boiling surface is assumed to completely depleted such that the contact line is normal to the boiling surface. Based on these assumptions, the surface tension forces acting at the liquid layer over the adiabatic confinement wall can be expressed as:

$$F_s = \epsilon\sigma, \tag{11}$$

where ϵ is the perimeter of the boiling surface. It is worth noting that the proposed CHF model assumes that the evaporating liquid microlayer is completely depleted at CHF such that the triple contact line is normal to the boiling surface. However, if this condition is not satisfied, the influence of the contact angle would be included in model fitting where the contact angle is a lumped with other fluid properties in one fitting parameter, ψ. Lastly, the hydrostatic force can be expressed in term of the effective depth of the interface, H_i, as follow:

$$F_G = H_i g(\rho_l - \rho_v)A_{gap}. \tag{12}$$

Critical heat flux is triggered when

$$F_M = F_s + F_G. \tag{13}$$

Combining Eqs. (10)–(13) yields an expression for CHF:

$$q''_{CHF,Co} = \sqrt{\frac{2\rho_v h_{lv}^2 A_{gap}(1 - \psi)}{A_b^2}\left(\epsilon\sigma + H_i g(\rho_l - \rho_v)A_{gap}\right)};$$
$$\left(\frac{q''_{CHF,Co}}{q''_{CHF,Z}} < 1\right). \tag{14}$$

The development of the confined CHF expression enables the prediction of the gap spacing threshold, below which confinement reduces the CHF compared to unconfined pool boiling. The predicted gap spacing threshold corresponds to the value where the confined CHF (Eq. (14)) matches the unconfined pool boiling CHF (Eq. (1)). Hence, the geometrical confinement effect on CHF can be indicated by the ratio between confined CHF and unconfined CHF:

$$\frac{q''_{CHF,Co}}{q''_{CHF,Z}} = \sqrt{\frac{2A_{gap}(1 - \psi)\epsilon}{K^2 A_b^2}\left(L_c + \frac{H_i A_{gap}}{\epsilon L_c}\right)}, \tag{15}$$

where K is the dimensionless unconfined CHF ratio defined in Eq. (1) and L_c is the capillary length of the working fluid. Boiling is considered unconfined when the confined CHF to the unconfined CHF ratio is larger than unity. Fig. A.1 illustrates the absolute mean error of the confined CHF model increases if the proposed cutoff is increased beyond the threshold values of unity. Thus, the model proposed here is deemed accurate for cases where the predicted CHF with confinement is lower than the CHF predicted for unconfined boiling.

To enumerate, the main assumptions employed to derive Eq. (14) are:

- The heated surface spans one side of the confinement gap.
- The opposing confinement wall is assumed to be adiabatic and completely wetted.
- The boiling gap spacing is smaller than the confinement threshold spacing indicated as a value of unity in Eq. (15).
- The two-phase interface where vapor generation occurs in the confined region is assumed to be at quasi-steady state.
- The ratio of the evaporation interface area to the confinement opening area, $(1 - \psi)$ is assumed to be dependent on the working fluid properties only.

The generic expression for CHF in Eq. (14) can be expressed for a particular geometry. For example, the CHF for a circular horizontal confined boiling surface of a diameter, D, and gap size, S, is

$$q''_{CHF,Co} = \sqrt{\frac{32\rho_v h_{lv}^2 S(1 - \psi)}{D^2}\left(\sigma + g\frac{S^2}{2}(\rho_l - \rho_v)\right)}. \tag{16}$$

Similarly, the CHF expression can be tailored to an inclined straight channel of length, L, uniform rectangular cross-sectional area with channel height, *i.e.,* gap size, S and channel width, W. When the channel is submerged in liquid pool with two openings at both ends of the channel and inclination angle, θ, where $\theta = 90°$ represents a vertical channel, the CHF can be expressed as:

$$q''_{CHF,Co} = \sqrt{\frac{8\rho_v h_{lv}^2 S(1 - \psi)}{L^2}\left(\sigma + g(SL\sin\theta + \frac{S^2}{2}\cos\theta)(\rho_l - \rho_v)\right)}. \tag{17}$$

4. Results and discussion

The confined pool boiling CHF model presented by Eq. (14) is compared to experimental data available from 10 distinct studies in the literature (Alsaati et al., 2021; Cardoso and Passos, 2012; Kapitz et al., 2015; Katto and Kosho, 1979; Nunes et al., 2020; Misale et al., 2011; Bonjour and Lallemand, 1997; Geisler and Bar-Cohen, 2009; Monde et al., 1982; Kim and Suh, 2003). To the best of our knowledge, this dataset comprises all the data that quantifies the effect the gap spacings on the CHF of confined pool boiling, in particular where there is an adiabatic wall parallel to the heated surface (and having the same
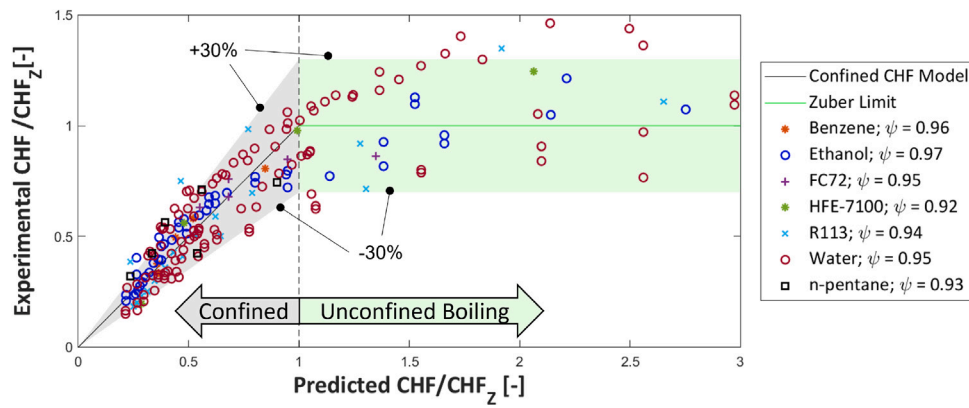
Fig. 3. Assessment of the proposed model for CHF in confined geometries. Both the experimental and predicted CHF are normalized by the prediction for the unconfined CHF from Zuber (1959). The solid black reference line indicates a perfect match, and the gray shaded region indicates $\pm 30\%$ from this reference line. This comparison is limited to a region where the proposed model is valid, namely, up to Zuber's limit for unconfined conditions (a value of 1 on the normalized axes). Thereafter, a green line indicates Zuber's limit and the shaded region illustrates $\pm 30\%$ around this limit. (For interpretation of the references to color in this figure legend, the reader is referred to the web version of this article.)

Table 2
Experimental data for CHF in confined geometry.

Working fluid	Shape	Geometry range	Reference
Water	Circular Horizontal	S = [0.2–2.2] mm; D = 25.4 mm	Alsaati et al. (2021)
n-pentane	Circular Horizontal	S = [0.1–0.5] mm; D = 12 mm	Cardoso and Passos (2012)
Water	Circular Horizontal	S = [0.1–0.3] mm; D = [5–20] mm	Kapitz et al. (2015)
Water, R113, Ethanol, Benzene	Circular Horizontal	S = [0.1–8] mm; D = [10–20] mm	Katto and Kosho (1979)
Water	Circular Horizontal	S = 0.1 mm; D = 20 mm	Nunes et al. (2020)
HFE-7100	Circular Horizontal	S = [0.5–3.5] mm; D = 30 mm	Misale et al. (2011)
R113	Rectangular Vertical Channel	S = [0.3–2.5] mm; L = 50 mm; W = 20mm	Bonjour and Lallemand (1997)
FC72	Rectangular Vertical Channel	S = [0.4–1] mm; L = 20 mm; W = 20 mm	Geisler and Bar-Cohen (2009)
Water, Ethanol	Rectangular Vertical Channel	S = [0.45–5] mm; L = [20–50] mm; W = 10 mm	Monde et al. (1982)
Water	Inclined Rectangular Channel	S = [1–2] mm; L = 35 mm; W = 15 mm; θ = [0–90]	Kim and Suh (2003)

area) that confines the boiling to the narrow gap formed between. All data are under atmospheric pressure conditions and for flat boiling surfaces without enhancement modifications such as porous coatings. This data set includes a total of 197 experimental measurement of CHF under confined conditions using various working fluids that include water, ethanol, FC-72, HFE-7100, R113, n-pentane, and benzene. In general, two confinement geometries are considered, circular horizontal confined boiling surfaces (Eq. (16)) and both vertical and inclined rectangular channels where heating is applied to one side of the channel and the entire channel is submerged in a liquid pool (Eq. (17)). Table 2 summarized the dataset including the ranges of confinement gap spacings.

As discussed in the confined CHF model development above, the ratio of the interface area to the confinement opening area, ψ, is an unknown assumed to depend on the working fluid. However, occurrences of viscous fingering (or Saffman-Taylor) instability has been reported in confined boiling configurations (Kapitz et al., 2015). Furthermore, the shape of the viscous fingering instability is strongly influenced by the density ratio of the two phases and the capillary number (the relative measure between viscous and surface tension) (Anjos et al., 2017). Hence, ψ is expected to be strongly influenced by the capillary number and the density ratio of the working fluid. In effect, the dataset is classified into subsets based on the working fluid. Then, estimated fluid-specific values for ψ are obtained through a least-squares fitting of the model predictions to the experimental datapoints within each subset. It is important to note that the fitting process excludes datapoints where the model predicts a CHF value larger than the Zuber pool boiling limit. The vapor area ratio is found to range from $0.92 < \psi < 0.97$ across various working fluids.

Fig. 3 compares the CHF model predictions to the experimental data points categorized by fluid type. Effectively, the predictive model is also able to predict the gap spacing threshold, below which confinement reduces the CHF compared to unconfined pool boiling, as

well as accurately predict this reduction of the CHF. The experimental and predicted values are both normalized against Zuber's limit for unconfined boiling (Eq. (1)). The proposed model accurately depicts the effect of confinement on CHF, as indicated by the agreement with the experimental data in the range of where the predictions are less than gap spacing threshold estimated by the Zuber limit ($q''_{\text{CHF,Co}} < q''_{\text{CHF,Z}}$). In this range, the predictions collapse within the gray-shaded region indicating $\pm 30\%$ from the experimental data. As expected, the model is not suitable when it predicts a CHF value larger than the Zuber limit ($q''_{\text{CHF,Co}} > q''_{\text{CHF,Z}}$). In this range, the experimental data are accurately predicted by Zuber's limit, with the data points collapsing into the green-shaded region indicating $\pm 30\%$ from Zuber's limit. In practice, the proposed model should be employed for accurate prediction of CHF only for gap spacings below the threshold, and above the threshold Zuber's limit should instead be used. Thus, the predicted threshold in the gap spacing separating the confined and unconfined boiling regimes thereby corresponds to approximately unity in the normalized predicted heat flux value ($q''_{\text{CHF,Co}}/q''_{\text{CHF,Z}}=1$) and the upper limiting gap spacing, S, can be determined as a function of system parameters from Eqs. (15)–(17). On the other hand, the proposed confined CHF model, Eq. (14), is validated with a dataset that includes gap sizes as small as 10% of the capillary length of the working fluid. Moreover, the model proposed is developed and limited to the cases where there is an adiabatic wall parallel to the heated surface (and having the same area) that confines the boiling to the narrow gap formed in between. A non-adiabatic confinement wall configuration would violate the assumption of the proposed model that the liquid layer over the confinement wall is preserved and not depleted at CHF. On the other hand, the model does not account for the thermofluidic impacts of the flow over unheated region in the case where the boiling surface is smaller than the confinement wall. Also, the model assumes an atmospheric pressure condition and a flat boiling surface without modification enhancement such as porous wicking coating.
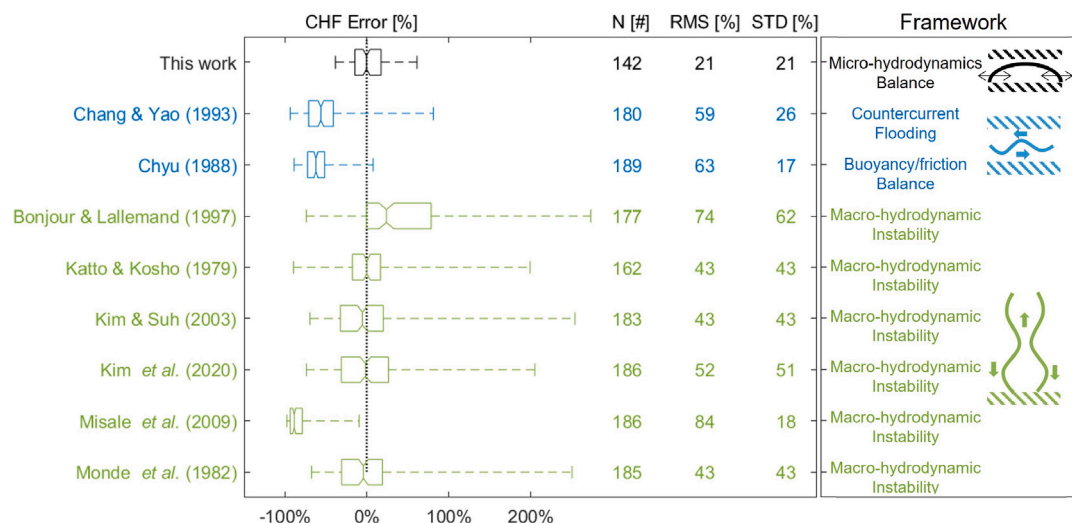
Fig. 4. Accuracy of the confined CHF models. The error is calculated by comparing the model to the experimental data points (N) in the dataset that are below the gap spacing threshold. The root mean square (RMS) and standard deviation (STD) of the prediction error for each model are tabulated within the plot. The notch in the box marks the mean error, whereas the box edges mark the 25th and the 75th percentiles. The dashed whiskers illustrate the full range of the calculated error in the data set. The results of the proposed model that is based on the micro-hydrodynamics balance in this work is shown in black in the first row, demonstrating low mean error and a narrow spread of the error compared to the models shown in subsequent rows that are based on alternative frameworks.

Fig. 4 compares the error in the prediction of CHF data for gap spacings below the threshold using the model developed in this work to other models in the literature, which are based on different triggering mechanism for CHF. The threshold gap spacing is defined uniquely for each model when the predicted CHF matches Zuber's limit for pool boiling. Several works (Bonjour and Lallemand, 1997; Katto and Kosho, 1979; Kim and Suh, 2003; Kim et al., 2020; Misale et al., 2009; Monde et al., 1982) based on the hydrodynamic instability framework are illustrated in green in Fig. 4. Despite having a low mean error, these models demonstrate the widest range of error among the tested models, indicating their lack of generality in predicting confined CHF across different geometries and fluid types. This is attributed to the fact that these models presume a CHF triggering mechanism that is associated with unconfined boiling when developing the empirical correlation.

The correlations of Change and Yao (1993) and Chyu (1988), highlighted in blue in Fig. 4, include the confinement effects on the hydrodynamics of the two-phase interface. This framework reduces the spread of error; however, both models drastically underestimate the CHF values on average. The model of Change and Yao (1993) postulates that CHF coincides with the countercurrent flooding phenomenon. Yet, there are experimental observations indicate the flooding, or partial dryout, occurs at heat fluxes lower that the CHF value (Alsaati et al., 2021; Bonjour and Lallemand, 1998; FujitaO et al., 1988). This explains the tendency of the model to underestimate the experimental CHF values in confined configurations. Similarly, the model of Chyu (1988), which is based on a friction framework, underestimates CHF values. This model assumes that the generated vapor traverses the entire confined space from the evaporation interface at the liquid inlet opening to the unconfined space through a vapor outlet opening. While this scenario can be correct in vertical channels, during confined boiling in a horizontal gap, the inlet and outlet openings are not well defined and generated vapor does not necessarily flow through the entire confined space.

The confined CHF model proposed in this work based on a micro-hydro-dynamics force balance, as marked in black in the top row, demonstrates both a very low mean error and narrow spread of error compared to other existing models. We believe the enhanced accuracy of this model is due to capturing the correct triggering mechanism for CHF in confined geometries. Specifically, the boiling crisis in confined geometries is caused by an imbalance of forces acting on the triple contact line that leads to irreversible growth of the dry spot on the boiling surface.

5. Conclusions

The boiling crisis in confined geometries has been previously described using empirical corrections made to models originally developed for unconfined geometries, which limits their accuracy outside a small range of applicability. To aid in engineering design, it is necessary to develop more generalized mechanistic CHF models for confined boiling. Therefore, it is critical to identify the triggering mechanism for CHF specific to boiling in these confined configurations. In this work, we developed a new mechanistic CHF model that accurately predicts the influence of confinement geometry on the boiling crisis. The model postulates that the insufficient liquid rewetting forces at the boiling surface edges are the triggering mechanism for CHF in confined geometries. A modeling framework was therefore developed based on the micro-hydrodynamics of the triple contact line on the boiling surface considering the competing vapor momentum, surface tension, and hydrostatic forces that govern the two-phase interface dynamics. Dryout is triggered when the vapor momentum force due to vaporization at the two-phase interface balances the combined surface tension and hydrostatic forces, leading to irreversible dryout of the surface.

The accuracy of the newly developed model is assessed by comparing to all available experimental data for confined CHF in the literature, consisting of 7 working fluids and a range of confinement gap spacings, heater sizes, shapes, and orientations. Notably, the model is able predict CHF for horizontal confined surfaces that have no clear distinction between liquid inlet and vapor outlet along the confinement perimeter. The model is able to predict the experimental CHF data with a root mean square error of 21% when the boiling dynamics are governed by confinement, a vast improvement compared to other confined CHF models available in the literature. The model is also able to identify the limit at which confinement no longer affects CHF, above which unconfined pool boiling CHF models should be used. In addition to offering a prediction tool for pool boiling CHF in confined conditions, this work provides a framework that can potentially be extended to include additional forces, such as liquid momentum forces, for predictions in flow boiling applications.

CRediT authorship contribution statement

Albraa A. Alsaati: Conceptualization, Data curation, Formal analysis, Investigation, Methodology, Software, Validation, Visualization, Writing – original draft, Writing – review & editing. **David M.**

Warsinger: Project administration, Resources, Supervision, Writing – review & editing. **Justin A. Weibel:** Conceptualization, Funding acquisition, Project administration, Resources, Supervision, Writing – review & editing. **Amy M. Marconnet:** Conceptualization, Funding acquisition, Project administration, Resources, Supervision, Writing – review & editing.

Declaration of competing interest

The authors declare that they have no known competing financial interests or personal relationships that could have appeared to influence the work reported in this paper.

Data availability
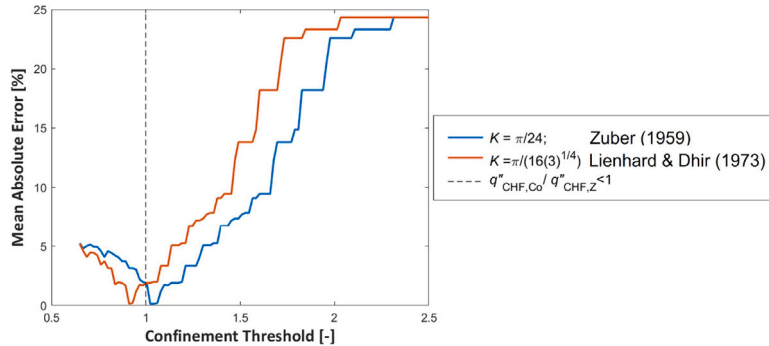
Data will be made available on request.

Fig. A.1. Sensitivity of the confinement threshold. The error is calculated by comparing the model for the confined CHF model (Eq. (14)) to the experimental data points in the dataset that are below the proposed confinement threshold limit (Eq. (15)). The vertical black dashed line corresponds to the confinement threshold of one where the confined CHF matches the unconfined CHF. The confinement threshold depends on the dimensionless unconfined CHF ratio, K. The error is calculated for two values of K found in the literature (blue and orange lines). In both cases, the minimum error is found near a ratio of one indicating that the cutoff in the applicability of the model is when the predicted CHF with confinement match the unconfined prediction. (For interpretation of the references to color in this figure legend, the reader is referred to the web version of this article.)
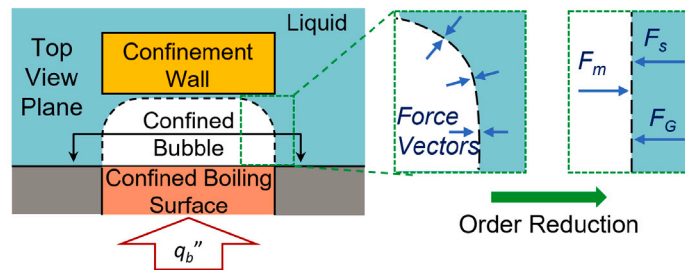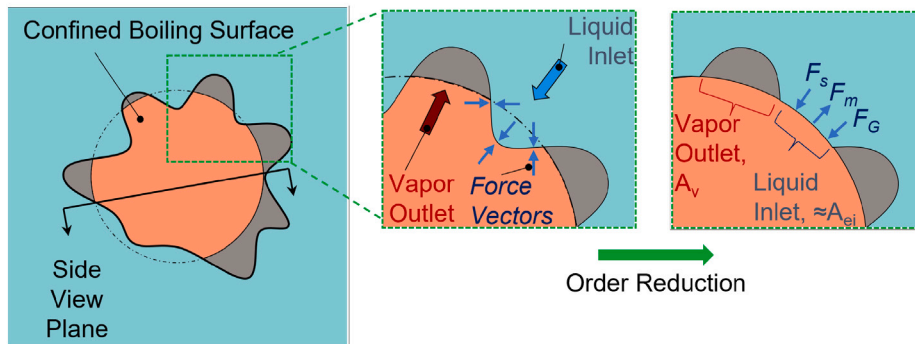

Fig. B.1. Model order reduction. An illustration of the model order reduction of the force balance. At the CHF condition, the model postulates that the vapor momentum forces, F_m, are balanced by surface tension, F_s, and hydrostatic pressure, F_G. While the confined vapor bubble has a complex three-dimensional shape, the model assumes that forces normal to the liquid inlet area dominate the boiling surface rewetting. Hence, the model dimensionality is reduced to enable a method for predicting critical heat flux with low computational cost.

Appendix A. Confinement threshold limit

See Fig. A.1.

Appendix B. Model order reduction

See Fig. B.1.

References

Alsaati, A., Warsinger, D., Weibel, J., Marconnet, A., 2021. Vapor stem bubbles dominate heat transfer enhancement in extremely confined boiling. Int. J. Heat Mass Transfer 177, 121520.

Anjos, P.H.A., Dias, E.O., Miranda, J.A., 2017. Radial fingering under arbitrary viscosity and density ratios. Phys. Rev. Fluids 2.

Arik, M., Bar-Cohen, A., 2001. Ebullient cooling of integrated circuits by novec fluids. In: Proceedings of the Pacific Rim International Intersociety Electronic Packaging Conference. pp. 18–32.

Bastakoti, D., Zhang, H., Li, D., Cai, W., Li, F., 2018. An overview on the developing trend of pulsating heat pipe and its performance. Appl. Therm. Eng. 141, 305–332.

Bellmann, R., Pennington, R.H., 1954. Effects of surface tension and viscosity on Taylor instability. Quart. Appl. Math. 21, 151–162.

Bonilla, C., Perry, C., 1941. Heat transmission to boiling binary liquid mixtures. Trans. Am. Soc. Chem. Eng. 37, 685–705.

Bonjour, J., Lallemand, M., 1997. Effects of confinement and pressure on critical heat flux during natural convective boiling in vertical channels. Int. Commun. Heat Mass Transfer 24, 191–200.

Bonjour, J., Lallemand, M., 1998. Flow patterns during boiling in a narrow space between two vertical surfaces. Int. J. Multiph. Flow. 24, 947–960.

Borishanskii, V., 1955. On the Problem of Generalizing Experimental Data on the Cessation of Bubble Boiling in Large Volume of Liquids. Report No. Ts. K.I.T 28, Moscow, Soviet Union.

Brandner, J., Anurjew, E., Bohn, L., Hansjosten, E., Henning, T., Schygulla, U., Wenka, A., Schubert, K., 2006. Concepts and realization of microstructure heat exchangers for enhanced heat transfer. Exp. Therm Fluid Sci. 30, 801–809.

Bruder, M., Bloch, G., Sattelmayer, T., 2016. Critical heat flux in flowboiling - Review of the current understanding and experimental approaches. Heat Transf. Eng. 38, 347–360.

Bucci, M., Richenderfer, A., Su, G.Y., McKrell, T., Buongiorno, J., 2016. A mechanistic IR calibration technique for boiling heat transfer investigations. Int. J. Heat Transfer 83, 115–127.

Cardoso, E.M., Passos, J., 2012. Nucleate boiling of n-pentane in a horizontal confined space. Heat Transf. Eng. 34, 470–478.

Carey, V.P., 2020. Liquid-Vapor Phase-Change Phenomena, third ed. Taylor and Francis, New York, NY.

Chang, Y., 1957. A theoretical analysis of heat transfer in natural convection and in boiling. Trans. ASME 79, 1501–1513.

Change, Y., Yao, S., 1993. Critical heat flux of narrow vertical annuli with closed bottoms. ASME J. Heat Transfer 105, 192–195.

Cheng, L., 2013. Fundamental issues of critical heat flux phenomena during flow boiling in microscale-channels and nucleate pool boiling in confined spaces. Heat Transf. Eng. 34, 1016–1043.

Chyu, M.C., 1988. Prediction of boiling dryout flux for restricted annular crevice. Int. J. Heat Mass Transfer 31, 1993–1998.

Coles, H., Herrlin, M., 2017. Immersion Cooling of Electronics in DoD Installation. Lawrence Berkeley National Laboratory, Berkeley, CA.

Devahdhanush, V., Mudawar, I., 2021. Review of critical heat flux (CHF) in jet impingement boiling. Int. J. Heat Mass Transfer 169, 120893.

El-Genk, M., Bostanci, H., 2003. Saturation boiling of HFE-7100 from a copper surface, simulating a microelectronic chip. Int. J. Heat Mass Transfer 46, 1841–1854.

FujitaO, Y., Ohta, H., Uchida, S., 1988. Nucleate boiling heat transfer and critical heat flux in narrow space between rectangular surfaces. Int. J. Heat Mass Transfer 31, 229–239.

Gambill, W., Lienhard, 1987. An upper bound for the critical boiling heat flux. In: ASME-JSME Thermal Engineering Joint Conference, Vol. 3. pp. 621–626.

Geisler, K., Bar-Cohen, A., 2009. Confinement effects on nucleate boiling and critical heat flux in buoyancy-driven microchannels. Int. J. Heat Mass Transfer 52, 2427–2436.

Harirchian, T., Garimella, S., 2009. The critical role of channel cross-sectional area in microchannel flow boiling heat transfer. Int. J. Multiph. Flow. 35.

Kandlikar, S., 2001. A Theoretical model to predict pool boiling CHF incorporating effects of contact angle and orientation. J. Heat Transfer 123, 1071–1079.

Kandlikar, S.G., 2012. History, advances, and challenges in liquid flow and flow boiling heat transfer in microchannels: A critical review. ASME. J. Heat Transfer 134, 034001.

Kapitz, M., Reinker, F., aus der Wiesche, S., 2015. Viscous fingering and heat transfer during boiling in a Hele–Shaw cell. Exp. Therm Fluid Sci. 67, 18–23.

Kapitz, M., Schmiedinghoff, L., Lüling, S.J., aus der Wiesche, S., 2019. Impact of surface parameters on confined boiling heat transfer in a Hele-Shaw cell. Heat Mass Transf. 55, 2533–02604.

Katto, Y., Kosho, Y., 1979. Critical heat flux of saturated natural convection boiling in a space bounded by two horizontal co-axial disks and heated from below. Int. J. Multiph. Flow. 5, 219–224.

Katto, Y., Yokoya, S., 1966. Experimental study of nucleate pool boiling in case of making interference-plate approach to the heating surface. In: Proceedings of 3rd International Journal of Heat Transfer Conference. Chicago, USA, pp. 219–227.

Katto, Y., Yokoya, S., Terakoa, K., 1977. Nucleate and transition boiling in a narrow space between two horizontal parallel disk surfaces. Bull. JSME 20, 638–643.

Kim, J., Jun, S., Laksnarain, R., You, S., 2016. Effect of surface roughness on pool boiling heat transfer at a heated surface having moderate wettability. Int. J. Heat Mass Transfer 101, 992–1002.

Kim, J., Shin, D., You, S., Lee, J., 2020. Pool boiling heat transfer on bare and microporous surfaces confined in a narrow gap. Int. J. Heat Mass Transfer 162, 120329.

Kim, Y.H., Suh, K.Y., 2003. One dimensional critical heat flux concerning surface orientation and gas size effects. Nucl. Eng. Des. 226, 277–292.

Kirichenko, Y., Chernyakov, P., 1971. Determination of the first critical thermal flux on flat heaters. J. Eng. Phys. Thermophys. 20, 699–703.

Konishi, C., Mudawar, I., 2015. Review of flow boiling and critical heat flux in microgravity. Int. J. Heat Mass Transfer 80, 469–493.

Lang, C., 1888. Transactions of institute of engineers and ship builders. Scotland 32, 279–295.

Liang, G., Mudawar, I., 2018a. Pool boiling critical heat flux (CHF) – Part 1: Review of mechanisms, models, and morrelations. Int. J. Heat Mass Transfer 117, 1352–1367.

Liang, G., Mudawar, I., 2018b. Pool boiling critical heat flux (CHF) – Part 2: Assessment of models and correlations. Int. J. Heat Mass Transfer 117, 1368–1383.

Liao, L., Bao, R., Liu, Z., 2008. Compositive effects of orientation and contact angle on critical heat flux in pool boiling of water. Heat Mass Transf. 44, 1447–1453.

Lienhard, J.H., Dhir, V.K., 1973. Extended hydrodynamic theory of the peak and minimum pool boiling heat fluxes. NASA CR-2270.

Lienhard, J., Dhir, V., Riherd, D., 1973. Peak pool boiling heat flux measurements on finite horizontal flat plates. ASME J. Heat Transf. 95, 477–482.

Misale, M., Guglielmini, G., Priarone, A., 2011. Nucleate boiling and critical heat flux of HFE-7100 in horizontal narrow spaces. Exp. Therm Fluid Sci. 35, 772–779.

Misale, M., Guglielmini, G., Priarone, A., Ambientale, C., 2009. HFE-7100 pool boiling heat transfer and critical heat flux in inclined narrow spaces. Int. J. Refrig. 32, 235–245.

Monde, M., Kusuda, H., Uehara, H., 1982. Critical heat flux during natural convective boiling in vertical rectangular channels submerged in saturated liquid. ASME J. Heat Transf. 104, 300–303.

Moon, J.H., Fadda, D., Shin, D.H., Kim, J.S., Lee, J., M.You, S., 2021. Boiling-driven, wickless, and orientation-independent thermal ground plane. Int. J. Heat Mass Transfer 167, 120817.

Nunes, J., deSouza, R., Rodrigues, A., Safaei, M., Cardoso, E.M., 2020. Influence of coated surfaces and gap size on boiling heat transfer of deionized water. J. Braz. Soc. Mech. Sci. Eng. 42, 127.

Pham, A., Barisik, M., Kim, B., 2013. Pressure dependence of Kapitza resistance at gold/water and silicon/water interfaces. J. Chem. Phys. 139.

Pollack, G., 1969. Kapitza Resistance. Rev. Modern Phys. 41, 48–81.

Ragland, W.A., Ganic, E.N., 1983. Flooding in counter-current two-phase flow. In: Kakaç, S., Ishii, M. (Eds.), Advances in Two-Phase Flow and Heat Transfer. Springer, Dordrecht, pp. 505–538.

Ramilison, J., Sadasivan, P., Lienhard, J., 1992. Surface factors influencing burnout on flat heaters. J. Heat Transfer 114, 287–290.

Souza, R.R., Passos, J.C., Cardoso, E.M., 2013. Confined and unconfined nucleate boiling under terrestrial and microgravity conditions. Appl. Therm. Eng. 51, 1290–1296.

Sundaram, A.S., Bhaskaran, A., 2011. Thermal modeling of thermosyphon integrated heat sink for CPU cooling. J. Electron. Cooling Therm. Control 1, 15–21.

Taylor, G.I., 1950. The instability of liquid surfaces when accelerated in a direction perpendicular to their plane. Proc. R. Soc. London. Ser. A, Math. Phys. Sci. 201.

Theofanous, T.G., Dinh, T.N., 2006. High heat flux boiling and burnout as microphysical phenomena: Mounting evidence and opportunities. Multiphase Sci. Technol. 18, 251–276.

Wallis, G.B., 1969. One-Dimensional Two-Phase Flow. McGraw Hill, New York, NY, USA.

Wang, L., Li, Y., Zhang, F., Xie, F., Ma, Y., 2016. Correlations for calculating heat transfer of hydrogen pool boiling. Int. J. Hydrogen Energy 41, 17118–17131.

Zhao, Y., Tsuruta, T., Masuoka, T., 2001. Critical heat flux of boiling heat transfer in a confined space. JSME Int. J. Ser. B 44, 344–351.

Zuber, N., 1959. Hydrodynamic aspects of boiling heat transfer. AEC Report AECU 4439.